Metabolism Clinical and Experimental 95 (2019) 93–101

Contents lists available at ScienceDirect

Metabolism Clinical and Experimental

journal homepage: www.metabolismjournal.com

Extracellular vesicles from human umbilical cord blood ameliorate bone loss in senile osteoporotic mice

Yin Hu [a,b], Ran Xu [h], Chun-Yuan Chen [a,b], Shan-Shan Rao [a,g], Kun Xia [a,b], Jie Huang [a,b], Hao Yin [a,b], Zhen-Xing Wang [a], Jia Cao [a], Zheng-Zhao Liu [a], Yi-Juan Tan [a], Juan Luo [a], Hui Xie [a,b,c,d,e,f,*]

[a] Movement System Injury and Repair Research Center, Xiangya Hospital, Central South University, Changsha, Hunan 410008, China
[b] Department of Orthopedics, Xiangya Hospital, Central South University, Changsha, Hunan 410008, China
[c] Department of Sports Medicine, Xiangya Hospital, Central South University, Changsha, Hunan 410008, China
[d] Hunan Key Laboratory of Organ Injury, Aging and Regenerative Medicine, Changsha, Hunan 410008, China
[e] Hunan Key Laboratory of Bone Joint Degeneration and Injury, Changsha, Hunan 410008, China
[f] National Clinical Research Center for Geriatric Disorders, Xiangya Hospital, Central South University, Changsha, Hunan 410008, China
[g] Xiangya Nursing School, Central South University, Changsha, Hunan 410013, China
[h] Department of Urology, The Second Xiangya Hospital, Central South University, Changsha, Hunan 410011, China

ARTICLE INFO

Article history:
Received 3 November 2018
Accepted 17 January 2019

Keywords:
Extracellular vesicles
Umbilical cord blood
Osteoporosis
miR-3960

ABSTRACT

Objective: Senile osteoporosis is one of the most common age-related diseases worldwide. Accumulating evidences have indicated that young blood can reverse age-related impairments. Extracellular vesicles (EVs) exert therapeutic effects in a variety of diseases by delivering bioactive molecules such as microRNAs (miRNAs). The aim of the study is to evaluate the therapeutic potential of EVs from human umbilical cord blood plasma (UCB-EVs) on senile osteoporosis and to preliminarily clarify the underlying mechanism.

Methods: UCB-EVs were injected into the tail vein of aged (16 months old) male C57BL/6 mice. Microcomputed tomography was performed to evaluate bone mass and microarchitecture of mice. The osteogenic and osteoclastic activities were determined by quantitative real-time PCR (qRT-PCR), histological examination and western blot analysis. *In vitro*, qRT-PCR assay was undertaken to explore the enrichment levels of a number of miRNAs that have positive effects in reducing bone loss. The efficacy of UCB-EVs on osteoblastic differentiation of bone marrow mesenchymal stromal cells (BMSCs) and osteoclastogenesis of RAW264.7 cells were assessed by cytochemical staining. Gene and protein expression changes were detected by qRT-PCR and western blotting respectively. Meanwhile, the roles of the selected miRNA in the regulatory effects of UCB-EVs on BMSCs and RAW264.7 cells were evaluated by using specific miRNA inhibitor.

Results: The intravenous injection of UCB-EVs for two months attenuated bone loss in old mice, as defined by increased trabecular and cortical bone mass, enhanced osteoblast formation and reduced osteoclast formation compared to the control mice. *In vitro*, UCB-EVs could promote the osteogenic differentiation of BMSCs and inhibit the osteoclastogenesis of RAW264.7 cells. Moreover, it was confirmed that miR-3960 was highly enriched in UCB-EVs and miR-3960 inhibitor reversed the stimulatory effect of UCB-EVs on osteoblastic differentiation of BMSCs.

Conclusion: Our findings indicate that UCB-EVs ameliorate age-related bone loss by stimulating bone formation and inhibiting bone resorption, and miR-3960 mediated the osteogenic effect of UCB-EVs on BMSCs. Thus, UCB-EVs may represent a promising agent for prevention of senile osteoporosis.

Abbreviations: UCB, umbilical cord blood; miRNAs, microRNAs; BMSCs, bone marrow mesenchymal stromal cells; EVs, extracellular vesicles; UCB-EVs, EVs from human umbilical cord blood plasma; TEM, transmission electron microscope; DLS, dynamic light scattering; μCT, microcomputed tomography; PFA, paraformaldehyde; ROI, region of interest; OCN, osteocalcin; TRAP, tartrate-resistant acid phosphatase; qRT-PCR, quantitative real-time PCR; ALP, alkaline phosphatase; ARS, alizarin red S; RANKL, receptor activator for nuclear factor-κB ligand; Runx2, runt-related transcription factor 2; COL1, type I collagen; NFATc1, nuclear factor of activated T cells c1; ATP6V0d2, ATPase H+ transporting V0 subunit d2; Ctsk, cathepsin K.

* Corresponding author at: Movement System Injury and Repair Research Center, Xiangya Hospital, Central South University, #87 Xiangya Road, Changsha, Hunan 410008, China.
E-mail address: huixie@csu.edu.cn (H. Xie).

https://doi.org/10.1016/j.metabol.2019.01.009
0026-0495/

1. Introduction

Osteoporosis is one of the most common metabolic bone diseases, affecting >200 million people throughout the world [1,2]. Old people living with osteoporosis usually suffer from a fragility fracture which will greatly affect the life quality of patients and increase the economic burden [3]. Senile osteoporosis is primarily associated with aging and caused by impaired bone formation [4,5]. Both bone formation of osteoblasts and bone resorption of osteoclasts involve in the physiological process of bone remodeling [6,7]. Thus, therapies designed to regulate the balance of bone remodeling hold significant potential for the prevention and treatment of osteoporosis.

Recently, exposure of aged animals to young blood has been widely studied for reversing age-related impairments. Accumulating evidences have demonstrated that young blood improves stem cell function of various tissues in aged animals, which is possibly caused by some beneficial factors from young blood [8–10]. Human umbilical cord blood (UCB), as one classical form of young blood, is supposed to also be able to rejuvenate the age-related dysfunction including senile osteoporosis, and has several unique advantages, such as easy accessibility, non-invasive to donors and no ethical concern [11]. However, the direct use of UCB for therapeutic purposes has the risks of immune rejection response, anaphylaxis and unpredicted cross-infection [12,13].

Extracellular vesicles (EVs), approximately 40–150 nm sized membrane-enclosed nanovesicles, are secreted by almost all cells for mediating intercellular communication *via* transferring bioactive molecules (nucleic acids, proteins and lipids) from source cells to target cells [14]. EVs possess anti-impairment and pro-regenerative effects in various disease models and have no obvious side effects [15]. Studies have shown that EVs released by mesenchymal stem cells can promote bone regeneration in critical-sized calvarial defects through enhancing osteogenesis of bone marrow mesenchymal stromal cells (BMSCs) [16–18]. Considering that UCB contains plenty of EVs [19], we assumed that EVs derived from human UCB (UCB-EVs) would have the ability to ameliorate age-related osteoporosis.

In this study, we firstly explored the effect of UCB-EVs on bone mass in aged mice. We also assessed the effects of UCB-EVs on osteogenesis and osteoclast formation *in vivo* and *in vitro*, and preliminarily clarified the underlying mechanism.

2. Materials and methods

2.1. Isolation and characterization of UCB-EVs

The isolation and characterization of UCB-EVs were performed as described previously [20,21]. Briefly, human UCB (50–60 mL per sample) was acquired from healthy full-term newborns with informed consent of the mother and permission of the Ethical Review Board at Xiangya Hospital of Central South University. The whole blood was collected from umbilical veins into the sterile bloodbag (Macopharma, France) containing anticoagulant of citrate phosphate dextrose with the first 2–3 mL of blood discarded. Blood samples were processed within 1 h of collection. The mixture was centrifuged to collect the plasma at 300 ×*g* for 10 min. Subsequently, the plasma underwent successive centrifugations (300 ×*g* for 10 min, 2000 ×*g* for 10 min, and 10,000 ×*g* for 30 min) to discard dead cells and cell debris. The final supernatant was ultracentrifuged for 70 min at 100,000 ×*g* within the same day and did not undergo freeze-thaw cycle. The pelleted EVs were washed with a large volume of PBS for twice and centrifuged at the same high speed, then re-suspended in 15 mL PBS. The EVs suspension was filtered through a 0.22 μm filter sterilizer (Millipore, Billerica, USA) and centrifuged at 4000 ×*g* to approximately 200 μL by ultrafiltration in a 15 mL Amicon Ultra-15 Centrifugal Filter Unit (Millipore). All procedures were performed at 4 °C. EVs were stored at −80 °C or used for the downstream experiments.

Transmission electron microscope (TEM) (Hitachi, Tokyo, Japan) and dynamic light scattering (DLS) with a Nanosizer™ instrument (Malvern Instruments, Malvern, UK) were used to observe the morphologies and measure the size distribution of UCB-EVs respectively. Flow cytometry was used to analyze the EV-characteristic surface marker proteins as described previously [20].

2.2. Animals and treatments

All animal experiments were approved by the Ethical Review Board at Xiangya Hospital of Central South University. 16-month-old male C57BL/6 mice (weighing 36–42 g) were used as senile osteoporosis model in this study. Mice were randomly divided into two groups, which were intravenously injected with UCB-EVs (100 μg dissolved in 100 μL PBS) or an equal volume of PBS through the tail vein for once a week. At 1, 2 and 8 weeks after the first treatment, the mice were sacrificed and bone specimens were harvested for further analysis.

2.3. Microcomputed tomography (μCT) analysis

μCT was used to quantitatively evaluate the bone mass. The right femora were dissected from mice, fixed for 48 h in 4% paraformaldehyde (PFA) and analyzed by high-resolution μCT (Skyscan, Aartselaar, Belgium). Voltage and current of the scanner were set to 50 kV and 400 μA, respectively, with a resolution of 8.88 μm per pixel. Cross-sectional images of distal femur were used to perform 3-dimensional histomorphometric analysis of trabecular bone. For trabecular bone, the region of interest (ROI) was drawn starting from 0.28 mm below the distal epiphyseal growth plate and extended proximally for 0.45 mm length to measure the trabecular bone volume fraction (Tb. BV/TV), trabecular thickness (Tb. Th), trabecular number (Tb. N) and trabecular separation (Tb. Sp). Cross-sectional images of the mid-diaphysis of femur were used to perform 3-dimensional histomorphometric analysis of cortical bone. For cortical bone, the ROI was selected in mid-diaphysis of the femur for a total of 5% of femoral length to measure the cortical thickness (Ct. Th), periosteal perimeter (Ps. Pm) and endosteal perimeter (Es. Pm).

2.4. Histochemical and immunohistochemical staining

The dissected femora were fixed in 4% PFA for 48 h, decalcified in 10% EDTA (pH 7.4) (Amresco, Solon, OH, USA) for 21 days and embedded in paraffin. 5-μm-thick longitudinally oriented bone sections were stained for osteocalcin (OCN) and tartrate-resistant acid phosphatase (TRAP) as previously described [22]. Anti-OCN and the secondary antibody were purchased from Takara Bios (Shiga, Japan). TRAP Staining Kit was purchased from Sigma (St. Louis, MO, USA). Images were photographed under an optical microscope. Relative staining intensity or positively stained cell number in distal metaphysis or diaphyseal endosteum of femora were measured in three random visual fields per section, three sequential sections per mouse and three mice in each group.

2.5. Cell culture

BMSCs were isolated from 4-week-old male wild-type mice. Briefly, bone marrow cells were flushed from the femora and suspended in α-MEM (Gibco, Grand Island, USA) containing 10% FBS (Gibco), 100 U/mL penicillin and 100 μg/mL streptomycin (Gibco). After 3 d, non-adherent cells were discarded and adherent cells were cultured, then passaged after reaching 80% confluence. BMSCs (passage 3–6) were used in the followed experiments. The mouse macrophage RAW264.7 was purchased from ATCC (Rockville, MD, USA) and cultured in high-glucose DMEM supplemented with 10% FBS, 100 U/mL penicillin and 100 μg/mL streptomycin. Cells were maintained at 37 °C with 5% CO_2 in a humidified environment.

2.6. EVs uptake assay

EVs were labeled with PKH67 fluorescent dye (Sigma) following the manufacturer's instruction. BMSCs or RAW264.7 cells were incubated with labeled EVs at 37 °C for 3 h and washed with PBS. Then, cells were fixed in 4% PFA for 15 min and washed with PBS for twice. Nuclei were stained with DAPI (0.5 μg/mL; Invitrogen, Carlsbad, USA). The green fluorescent signals were detected by a fluorescence microscope (Leica DMI6000B, Solms, Germany). To determine the uptake of EV-derived miRNAs, BMSCs or RAW264.7 cells were treated with EVs for 3 h and then collected to analyze the expression of miRNAs by quantitative real-time PCR (qRT-PCR).

2.7. Cell transfection

MiR-3960 inhibitor and negative control inhibitor were purchased from RiboBio (Guangzhou, China). As previously described [20], the cells were cultured in 6-well plate until reaching 90% confluency, then transfected with miR-3960 inhibitor or the negative control inhibitor using Lipofectamine 2000 (Invitrogen), and incubated with 100 μg/mL UCB-EVs or an equal volume of PBS. After 24 h, the downstream experiments were performed.

2.8. Osteogenic differentiation assay

BMSCs were plated in 48-well plates at 1.0×10^5 cells per well. After 24 h, the cells were cultured in osteogenesis induction medium (Cyagen Biosciences Inc., Santa Clara, USA) treated with or without UCB-EVs (100 μg/mL) and miR-3960 inhibitor. The medium was changed every three days. After 3 days of induction, the differentiated BMSCs were washed with PBS, fixed in 4% PFA for 10 min, and then assayed with an Alkaline Phosphatase (ALP) Staining Kit (Beyotime, Shanghai, China). After 14 days of induction, the cells were washed with PBS, fixed in 4% PFA for 10 min, and then stained with 2% Alizarin Red S (ARS) solution (Solarbio, Beijing, China) at pH 4.2. An inverted microscope (Leica DMI6000B, Solms, Germany) was used for imaging. The expression of osteogenesis-related genes and proteins was analyzed by qRT-PCR and western blot respectively.

2.9. Osteoclast differentiation assay

RAW264.7 cells were plated in 48-well plates at 1.5×10^4 per well. After 24 h, the cells were cultured in high glucose DMEM containing 100 ng/mL receptor activator for nuclear factor-κB ligand (RANKL; Peprotech, London, England) treated with or without UCB-EVs (100 μg/mL) and miR-3960 inhibitor. The medium was changed every three days. After 8 days of induction, the cells were washed with PBS and fixed in 4% PFA for 10 min. Osteoclasts were stained using a commercially TRAP Kit (Sigma) and then quantified using an inverted microscopy (Leica). The expression of osteoclastogenesis-related genes and proteins was analyzed by qRT-PCR and western blot respectively.

2.10. qRT-PCR analysis

Total RNA from cultured cells or femur tissues was extracted using Trizol Reagent (Invitrogen). For mRNA analysis, cDNA was synthesized from 1 μg total RNA by using a Revert Aid First-strand cDNA Synthesis Kit (Fermentas, Life Sciences, Canada). Then, amplification reactions were performed with FastStart Universal SYBR Premix ExTaq™ II (Takara Biotechnology, Japan) in an ABI PRISM® 7900HT System (Applied Biosystems, Foster City, USA). Relative mRNA expression was calculated by the relative standard curve method ($2^{-\Delta\Delta CT}$) with GAPDH as the reference. The PCR primers used in this study were as follows: runt-related transcription factor 2 (*Runx2*): forward, 5′-GACTGTGGTTACCG TCATGGC-3′, and reverse, 5′-ACTTGGTTTTTCATAACAGCGGA-3′; *Alpl*: forward, 5′-CCAACTCTT TTGTGCCAGAGA-3′, and reverse, 5′-GGCTAC ATTGGTGTTGAGCTTTT-3′; *Bglap*: forward, 5′-CTGACCTCACAGATCC CAAGC-3′, and reverse, 5′-TGGTCTG ATAGCTCGTCACAAG-3′; alpha 1 type I collagen (*Col1a1*): forward, 5′-GACATG TTCAGCTTTGTGGACC TC-3′, and reverse, 5′-GGGACCCTTAGGCCATTGTGT A-3′; *Trap*: forward, 5′-TGGTCCAGGAGCTTAACTGC-3′, and reverse, 5′-GTCAG GAGTGGGAG CCATATG-3′; nuclear factor of activated T cells c1 (*Nfatc1*): forward, 5′-CAGTGTGACCGAAGATACCTGG-3′, and reverse, 5′-TCGAGACTTGA TAGG GACCCC-3′; ATPase H+ transporting V0 subunit d2 (*Atp6v0d2*): forward, 5′-AGCA AAGAAGACAGGGAG-3′, and reverse, 5′-CAGCGT CAAACAAAGG-3′; cathepsin K (*Ctsk*): forward, 5′-GCGGCATTACCAAC AT-3′, and reverse, 5′-CTGGAAGCAC CAACGA-3′; *Gapdh*: forward, 5′-CACCATGGAGAAGGCCGGGG-3′, and reverse, 5′-GACGGACACATTGG GGGTAG-3′. For miRNA detection, total EV-derived miRNAs were isolated using the SeraMir Exosome RNA Purification Kit (System Biosciences, Mountain View, USA), and cDNA for miRNAs was synthesized using the Mir-X™ miRNA First-Strand Synthesis Kit (Takara) according to the manufacturer's protocol. Amplification reactions were performed using a miRNA SYBR Green qRT-PCR Kit (Takara) with the provided universal reverse primer and miRNA reference gene U6. The miRNA-specific forward primers were synthesized by Sangon Biotech (Shanghai, China).

2.11. Western blot analysis

Western blotting was carried out as described previously [20]. Total proteins were extracted from cultured cells or femur tissues using RIPA lysis buffer supplemented with protease inhibitor cocktail (Sigma). Extracted proteins were separated by sodium dodecyl sulfate-polyacrylamide gel electrophoresis (SDS-PAGE) and then transferred to polyvinylidene fluoride membranes (Millipore). The membranes were blocked with 5% non-fat milk for 2 h and then probed with primary antibodies at 4 °C overnight. Subsequently, the membranes were incubated with horseradish peroxidase (HRP)-conjugated secondary antibodies at 37 °C for 1 h at room temperature. The antibodies including anti-RUNX2, anti-OCN, anti-NFATc1, anti-Ctsk, anti-β-actin, and HRP-conjugated secondary antibodies were obtained from Santa Cruz Biotechnology (Dallas, Texas, USA). The immunoreactive bands were visualized using a chemiluminescence reagent (Thermo Fisher Scientific, Waltham, USA) and imaged by the ChemiDoc XRS Plus luminescent image analyser (Bio-Rad).

2.12. Statistical analysis

Data are shown as means ± standard deviation (SD). Means between two groups were compared by 2-tailed Student's *t*-test. Statistical analysis was conducted using GraphPad Prism software and $P < 0.05$ was considered statistically significant.

3. Results

3.1. Characterization of UCB-EVs

TEM, DLS analysis and flow cytometric analysis were used to characterize the vesicles derived from UCB. The results showed that the majority of these particles exhibited a characteristic cup- or sphere-shaped morphology with a diameter ranging from 30 nm to 100 nm (Fig. 1A–B), similar to previously reported EVs [23]. Moreover, these particles showed the presence of surface markers such as CD63 and TSG101 (Fig. 1C), which further confirmed their EV identity.

3.2. UCB-EVs prevent age-associated bone loss in mice

To investigate the roles of UCB-EVs on senile osteoporosis, 16-month-old mice were injected with UCB-EVs or an equal volume of EVs diluent (PBS) through the tail vein. μCT scanning showed that

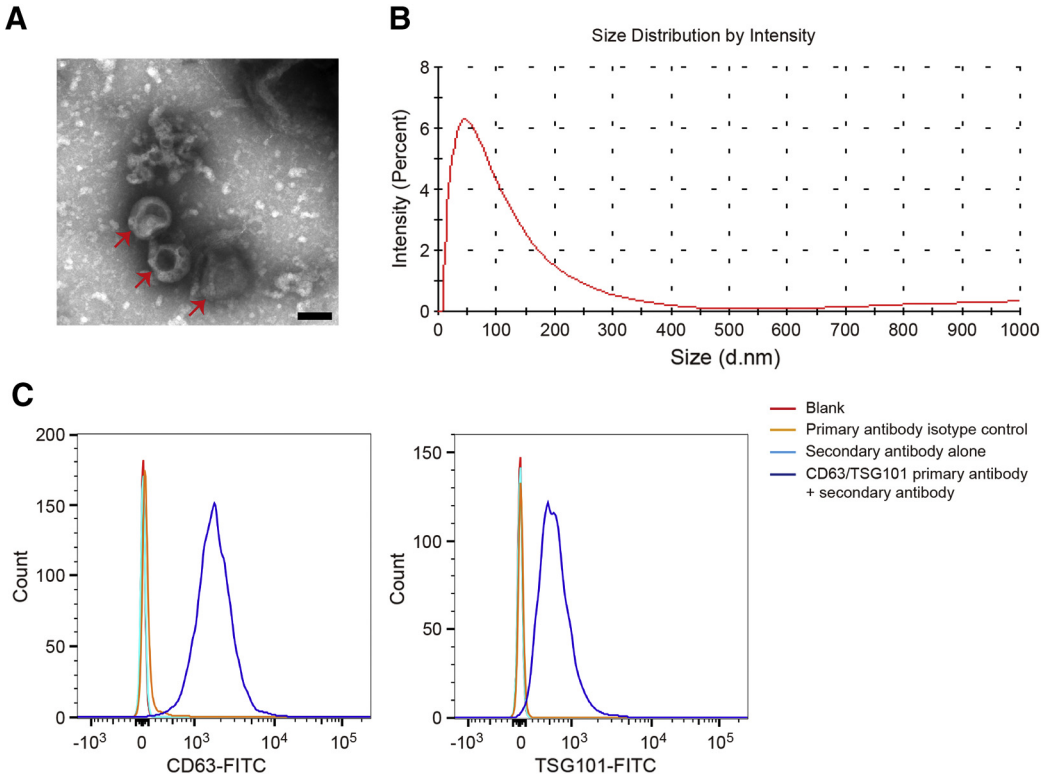

Fig. 1. Characterization of UCB-EVs. (A) TEM micrograph of UCB-EVs. Scale bar: 50 nm. (B) UCB-EVs size distribution measured by DLS analysis. (C) Flow cytometry analysis of the EV surface markers (CD63 and TSG101) on UCB-EVs. Blank: EVs incubated without antibody.

trabecular and cortical bone mass were higher in the femur of EVs-treated mice compared to the PBS-treated control mice after 2 months of administration (Fig. 2A). Quantitative analysis revealed that the trabecular bone volume fraction, thickness and number increased and the trabecular separation decreased in mice treated with UCB-EVs relative to the control group (Fig. 2B–E). The cortical bone thickness increased and the endosteal perimeter remarkably decreased in EVs-treated group relative to the control group (Fig. 2F–H). These data indicate that UCB-EVs treatment results in the reduction of bone loss in mice.

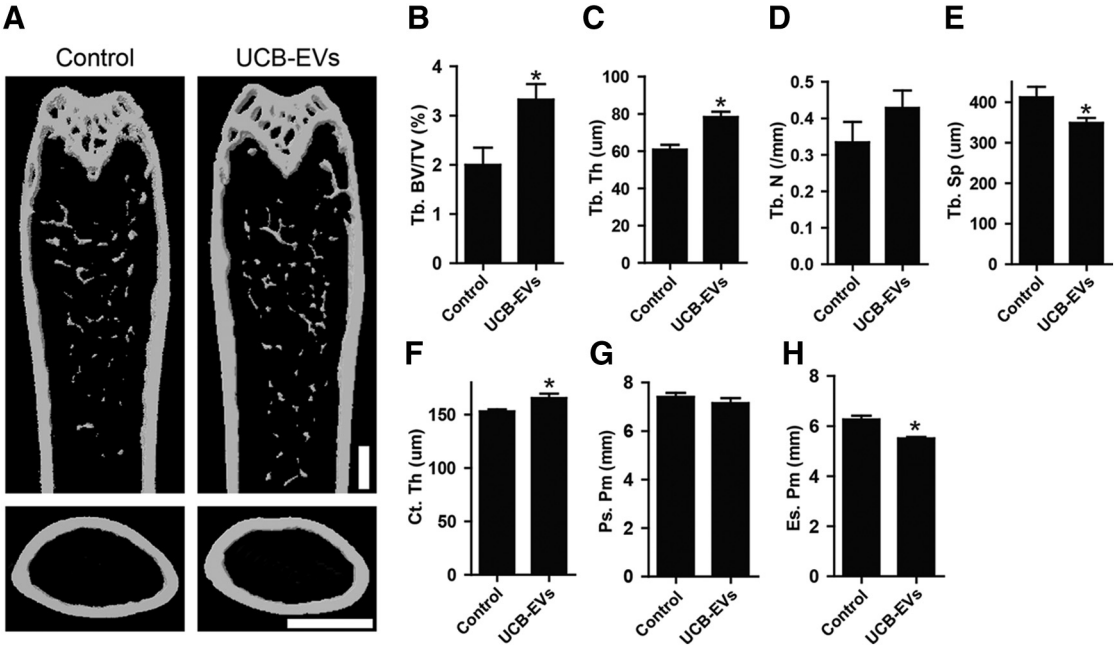

Fig. 2. UCB-EVs transplantation attenuates bone loss in age-associated osteoporotic mice. (A) Representative μCT 3D reconstruction images of femora from UCB-EVs- or PBS-treated 18-month-old mice. Scale bar: 1 mm. (B–H) Quantitative analyses of trabecular and cortical bone microarchitecture in femora. $n = 5–6$ per group. Tb. BV/TV, trabecular bone fraction; Tb. Th, trabecular thickness; Tb. N, trabecular number; Tb. Sp, trabecular separation; Ct. Th, cortical thickness; Ps. Pm, periosteal perimeter; Es. Pm, endosteal perimeter. $^*P < 0.05$ compared with the PBS group.

3.3. UCB-EVs promote osteogenesis and inhibit osteoclastogenesis in vivo

We then determined whether UCB-EVs exerted bone-sparing effect by regulating the osteogenic and osteoclastic activities. qRT-PCR analysis showed that the expression of osteogenesis-related genes including *Runx2*, *Bglap* and *Col1a1* was up-regulated and the expression of osteoclastogenesis-related genes including *Trap*, *Nfatc1*, *Ctsk* was down-regulated in UCB-EVs-treated mice compared with the control mice after 2 months of administration (Fig. 3A–C, G–I). Immunostaining and western blot were also performed to examine the expression levels of bone related proteins *in vivo*. As shown in Fig. 3D–E, the intensity of OCN staining on the trabecular bone surface in EVs-treated mice was enhanced compared to the control mice. TRAP staining revealed that the numbers of osteoclast on both trabecular and endosteal bone surfaces were markedly decreased after UCB-EVs treatment (Fig. 3J–L). Consistent with the above findings, the results of western blotting further confirmed the increase of osteogenic responses and the decrease of osteoclastic activities in bone tissues induced by EVs at 2 months post-treatment (Fig. 3F). This difference in the protein expression levels of bone tissues between UCB-EVs-treated mice and the control mice could also be detected at 2 weeks post-treatment before bone mass increased, but it was not observed at 1 week post-treatment (Supplementary Fig. 1). Taken together, our *in vivo* functional studies suggested that UCB-EVs prevented age-associated bone loss through the regulation of osteogenesis and osteoclastogenesis.

3.4. Detection of miRNAs in UCB-EVs

To explore the key molecules that mediate the therapeutic potential of UCB-EVs on age-related osteoporosis, qRT-PCR analysis was used to detect the levels of a class of miRNAs in UCB-EVs, including miR-3960, miR-146a, miR-34a, miR-503, miR-218 and miR-26a, which have been reported to promote osteogenesis and/or inhibit osteoclastogenesis [24–26]. The data demonstrated that the concentration of miR-3960

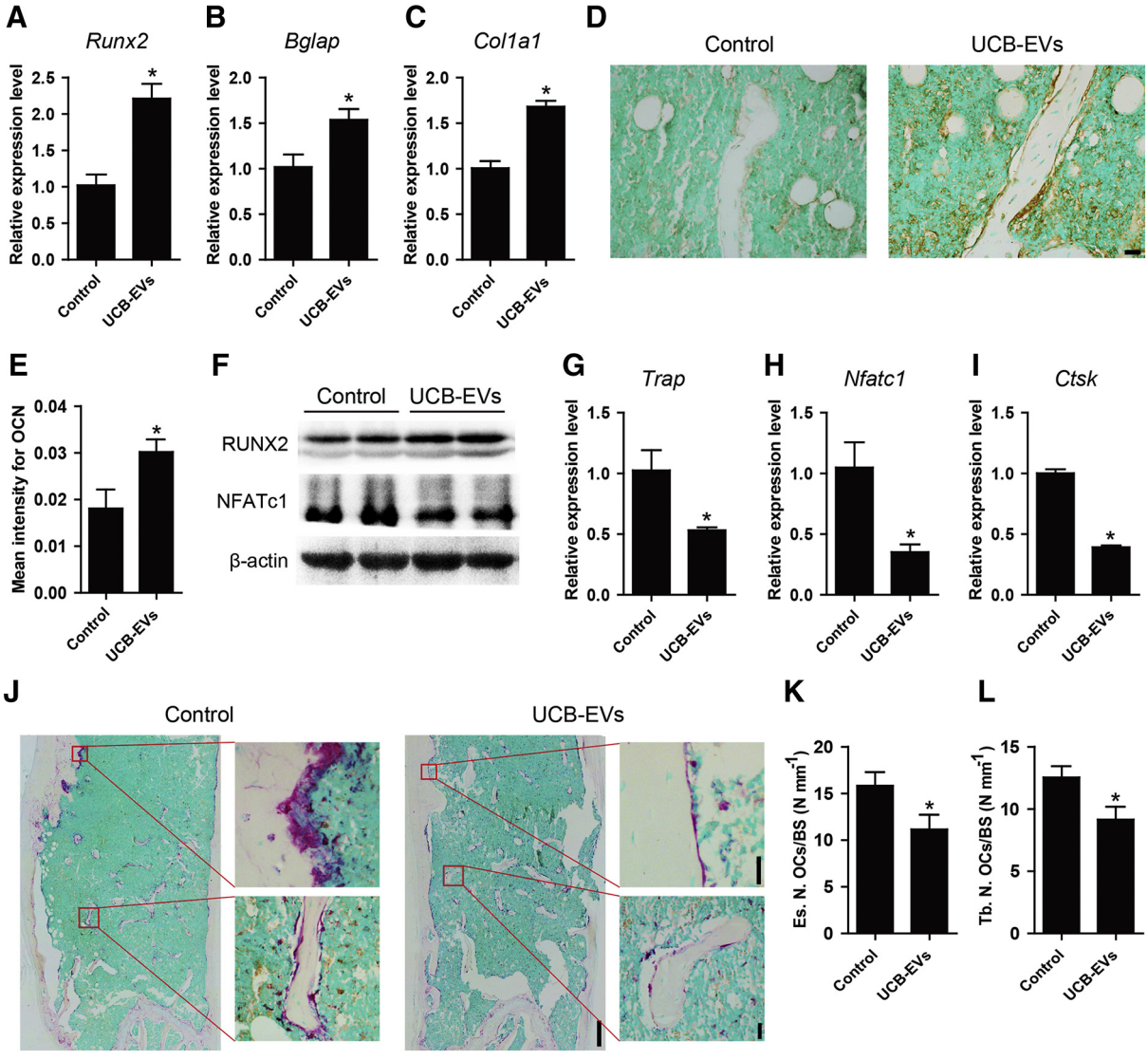

Fig. 3. Aged mice treated with UCB-EVs exhibit increased osteogenic activities and decreased osteoclastic activities. (A–C) The expression levels of osteogenesis-related genes including *Runx2*, *Bglap* and *Col1a1* in femur tissues from UCB-EVs- or PBS-treated 18-month-old mice were assessed by qRT-PCR. $n = 3$ per group. (D) Representative images of OCN immunohistochemical staining in distal femora from aged mice treated with UCB-EVs or PBS. Scale bar: 20 μm. (E) Quantification of the mean intensity of positively stained areas in (D). $n = 9$ per group. (F) The protein levels of RUNX2 and NFATc1 measured by western blotting in femur tissues from aged mice after 2 months of administration of UCB-EVs or PBS. (G–I) The mRNA expression levels of *Trap*, *Nfatc1* and *Ctsk* were evaluated by qRT-PCR analyses in femur tissues from UCB-EVs-treated mice and the control mice. $n = 3$ per group. (J) Representative TRAP staining images of femora from aged mice treated with UCB-EVs or PBS. Scale bars: 250 μm (left), 20 μm (right). (K–L) Quantification of the number of osteoclasts (N. OCs) on endosteal (Es) bone surface (BS) of diaphysis (K) and trabecular (Tb) bone surface of distal metaphysis (L) in (J). $n = 10$ per group. $^*P < 0.05$ compared with the PBS group.

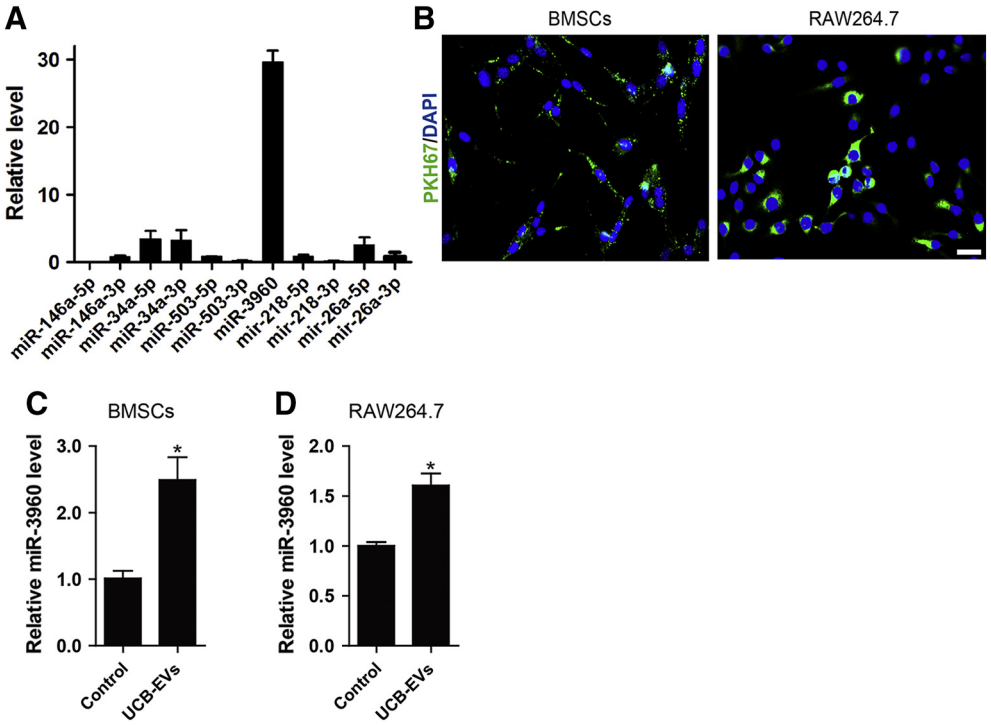

Fig. 4. UCB-EVs transfer miR-3960 into osteoblasts and osteoclasts. (A) qRT-PCR analysis of the enrichment of the miRNAs in UCB-EVs. n = 3 per group. (B) Representative fluorescence images of PKH67-labeled UCB-EVs (green) uptake by BMSCs and RAW264.7. Scale bar: 50 μm. (C–D) Detection of the level of miR-3960 in BMSCs and RAW264.7 cells incubated with UCB-EVs for 3 h. $n = 3$ per group. $^{*}P < 0.05$ compared with the control group.

was much higher compared with other miRNAs (Fig. 4A). Our previous studies have indicated that miR-3960 can not only promote osteogenesis of mouse ST2 stromal cells [26], but also enhance the osteogenic transdifferentiation of vascular smooth muscle cells [27]. Thus, we focused on EV-derived miR-3960 for further investigation.

3.5. UCB-EVs deliver miR-3960 into osteoblasts and osteoclasts

To detect whether UCB-EVs could be taken up by osteoblasts and osteoclasts *in vitro*, UCB-EVs were labeled with the PKH67 dye (green fluorescence) and then incubated with BMSCs and RAW264.7 cells for 3 h. As shown in Fig. 4B, the PKH67-labeled EVs were found in the cytoplasm of BMSCs and RAW264.7 cells. We next determined the transfer of miR-3960 into recipient cells. After treatment with UCB-EVs for 3 h, BMSCs and RAW264.7 cells were harvested. qRT-PCR analysis demonstrated that miR-3960 levels in BMSCs and RAW264.7 cells were remarkably increased after incubation with UCB-EVs (Fig. 4C–D). The results suggest that miR-3960 can be shuttled into target cells by UCB-EVs.

3.6. UCB-EVs promote osteoblast differentiation via transferring miR-3960

To evaluate the effects of UCB-EVs on osteoblasts *in vitro*, BMSCs were cultured in osteogenesis induction medium supplemented with UCB-EVs or an equal volume of PBS. ALP and ARS staining were performed to determine the osteoblastic differentiation of BMSCs after 3 and 14 days of induction, respectively. As illustrated in Fig. 5A–D, the EV-treated BMSCs showed enhanced ALP activity and matrix mineralization than the control group. To verify the role of miR-3960 in the EVs-induced regulation of BMSCs, a specific inhibitor targeting miR-3960 was used to interfere with the UCB-EVs-treated BMSCs. The results revealed that the pro-osteogenic ability of UCB-EVs was attenuated in the UCB-EVs + miR-3960 inhibitor group. qRT-PCR demonstrated that UCB-EVs treatment caused a significant increase in the expression of osteogenesis-related genes including *Runx2*, *Alpl*, *Bglap* and *Col1a1*, whereas inhibition of miR-3960 markedly reduced the effects (Fig. 5E–H). The expression levels of osteogenesis-related proteins in BMSCs receiving different treatments were also assessed by western blot. As shown in Fig. 5I, the miR-3960 inhibitor markedly reversed the UCB-EVs-induced up-regulation of the protein levels of RUNX2 and OCN in BMSCs. Our results suggest that miR-3960 mediates the osteogenic effect of UCB-EVs.

3.7. UCB-EVs inhibit osteoclast differentiation

Subsequently, we explored whether UCB-EVs could influence osteoclast formation and the role of miR-3960 in this process. TRAP staining showed that UCB-EVs remarkably inhibited osteoclastic differentiation of RAW264.7 cells induced by RANKL, while the effect couldn't be impaired by co-treatment with the miR-3960 inhibitor (Fig. 6A–B). qRT-PCR analysis was also performed to assess the mRNA levels of osteoclastogenesis-related genes including *Trap*, *Nfatc1*, *Atp6v0d2*, *Ctsk*. The results revealed that the expression of these genes was markedly down-regulated in the differentiated RAW264.7 cells after UCB-EVs stimulation compared with the control (Fig. 6C–F). UCB-EVs-induced down-regulation of these genes was not affected by the miR-3960 inhibitor (Fig. 6C–F). Western blotting was carried out to detect the levels of osteoclastogenesis-related proteins. Compared to the control, incubation with UCB-EVs resulted in a remarkable decrease in the protein expression levels of NFATc1 and Ctsk in RAW264.7 cells (Fig. 6G). However, the inhibitory effect of EVs was not impaired after the RAW264.7 cells were cultured with the miR-3960 inhibitor. All the data indicate that UCB-EVs can inhibit osteoclast differentiation.

4. Discussion

The balance of bone resorption and bone formation is essential for maintenance of bone mass [4]. Senile osteoporosis, a common age-related degenerative disease caused by uncoupling of bone resorption and bone formation, is characterized by a low bone turnover state with reduced bone formation [28]. In our present study, we demonstrated that intravenous injection of UCB-EVs could effectively alleviate age-related bone loss in old mice, as defined by increased trabecular and cortical bone mass, enhanced osteogenic

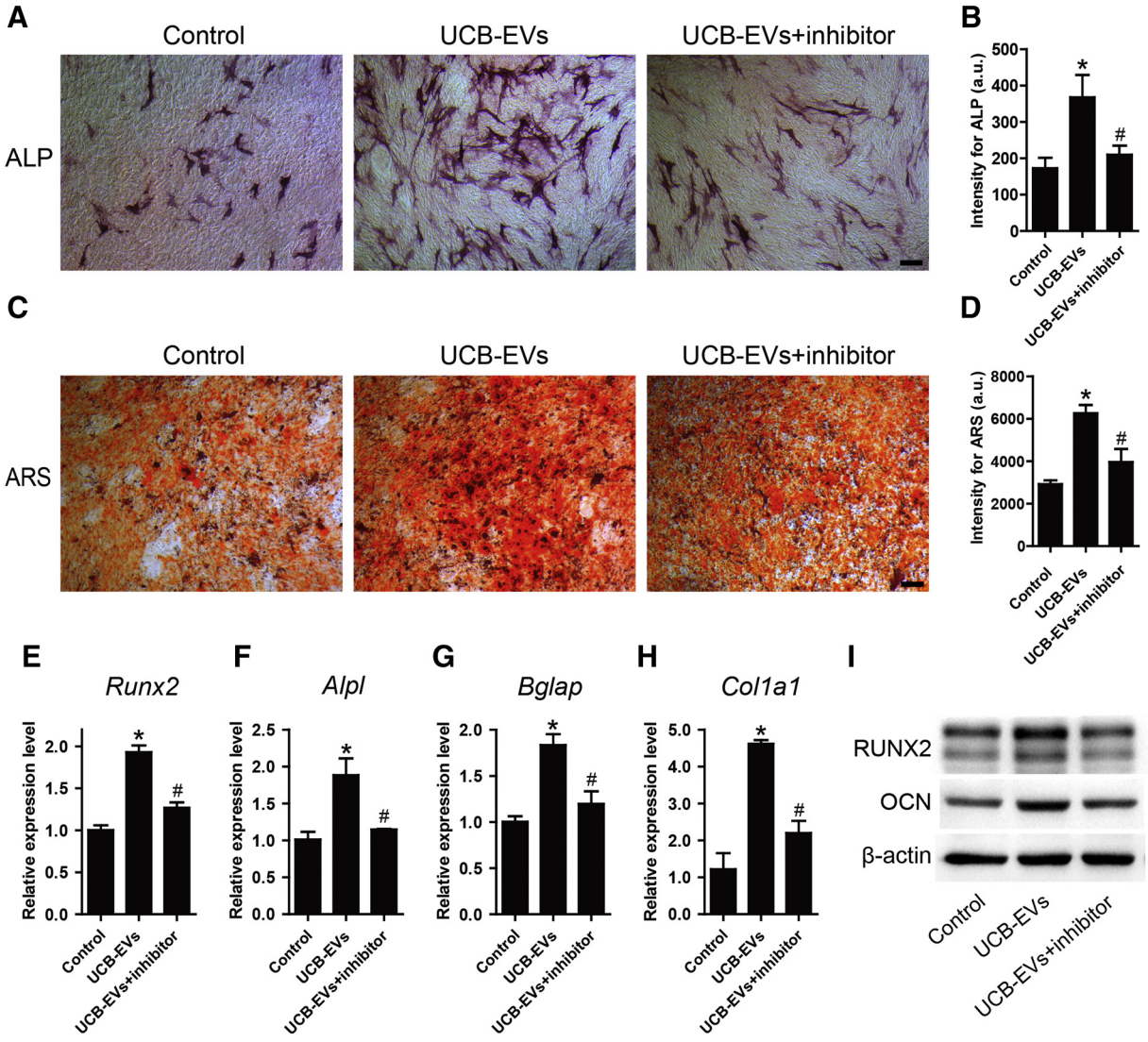

Fig. 5. UCB-EVs promote osteogenic differentiation of BMSCs *via* transferring miR-3960. BMSCs were cultured in osteogenesis induction medium treated with PBS + negative control inhibitor, UCB-EVs + negative control inhibitor, or UCB-EVs + miR-3960 inhibitor. (A–D) Representative images of alkaline phosphatase staining (A) and alizarin red S staining (C) and quantification of the staining intensity (B, D). Scale bar: 100 μm. $n = 5$ per group. (E–H) The expression levels of osteogenesis-related genes including *Runx2*, *Alpl*, *Bglap* and *Col1a1* in BMSCs on day 3. n = 3 per group. (I) The expression levels of osteogenesis-related proteins including RUNX2 and OCN examined by western blotting on day 7. $^{*}P < 0.05$ compared with the control group, $^{\#}P < 0.05$ compared with the UCB-EVs (100 μg/mL) group.

activities and reduced osteoclast formation. We also showed that UCB-EVs promoted osteoblast formation and inhibit osteoclast formation *in vitro*. Moreover, we found that miR-3960 was abundant in UCB-EVs and mediated the regulatory effect of UCB-EVs on osteoblast differentiation.

Over the past years, the application of multipotent stem cells for bone tissue engineering has received much attention among researchers and clinicians [29–31]. UCB is one of the most plentiful reservoir of stem cells and UCB-derived stem cells have therapeutic potential for many diseases including osteoporosis [11,32,33]. Recent studies have demonstrated that transplantation of stem cells contributes to tissue repair and regeneration not by the direct differentiation into the parenchymal cells that repairs the damaged tissues, but rather by the paracrine mechanisms to regulate the activity of resident tissue cells [34,35]. EVs are crucial paracrine mediators obtained from most cells and biological fluids including plasma. Stem cells-derived EVs possess therapeutic effects in various disease models similar to their original cells [15], suggesting that EVs are critical effectors of stem cells. Qi et al. indicated that EVs released by human-induced pluripotent stem cell-derived MSCs promoted bone regeneration of critical-sized calvarial defects in osteoporosis rat [16]. Furuta et al. reported that EVs derived from BMSCs could accelerate the process of fracture healing [36]. These results provided evidences that EVs could be used to stimulate bone repair in osteoporosis. UCB contain abundant EVs other than stem cells [19]. A large number of studies have reported the function of UCB-derived stem cells on tissue regeneration [11], whereas few studies have directly utilized UCB to extract EVs for therapeutic uses. Our previous studies showed that UCB-EVs effectively promoted cutaneous wound healing in mice [20]. Herein, we harvested EVs from human UCB plasma and verified that UCB-EVs could ameliorate bone loss in trabecular and cortical bone of senile osteoporotic mice, indicating that UCB-EVs might be utilized as a new agent for prevention or treatment of osteoporosis.

Decreased bone formation is the principal pathophysiological mechanism of senile osteoporosis [5]. BMSCs are the major source of osteoblasts that contribute to bone formation [37]. The age-associated attenuation of osteoblast activity is attributed to the weakened osteogenic differentiation potential of BMSCs in elderly subjects [37]. In this study, we demonstrated that UCB-EVs could be uptaken by BMSCs and remarkably accelerated osteoblastic differentiation of BMSCs, as

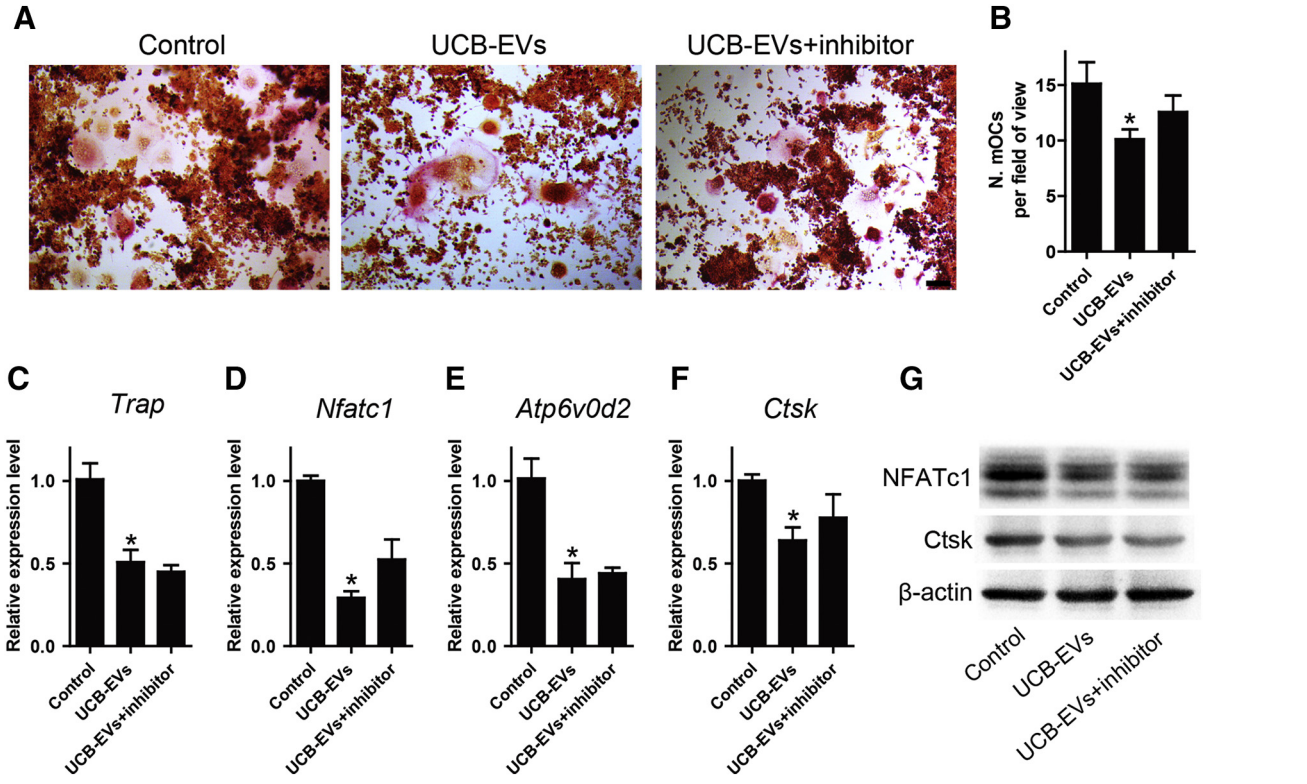

Fig. 6. UCB-EVs inhibit osteoclast differentiation of RAW264.7 cells. Raw264.7 cells were cultured in RANKL-containing medium supplemented with PBS + negative control inhibitor, UCB-EVs + negative control inhibitor, or UCB-EVs + miR-3960 inhibitor. (A) Representative images of TRAP staining. Scale bar: 100 μm. (B) Quantification of the number of TRAP positive multinucleated cells in (A). $n = 9$ per group. (C–F) The expression levels of *Trap*, *Nfatc1*, *Atp6v0d2* and *Ctsk* in Raw264.7 cells. n = 3 per group. (G) The expression levels of osteoclastogenesis-related proteins including NFATc1 and Ctsk detected by western blotting on day 6. $^*P < 0.05$ compared with the control group.

defined by increased ALP activity and matrix mineralization, as well as enhanced expression levels of osteogenesis-related genes and proteins, in consistent with our *in vivo* data showing increased osteogenic responses. Other than promotion of osteogenesis, UCB-EVs could also inhibit osteoclastogenesis, as evidenced by decreased number of osteoclasts and reduced expression levels of osteoclastogenesis-related genes and proteins. Therefore, the beneficial effects of UCB-EVs on senile osteoporosis may be ascribed to their function in regulation of endogenous osteoblasts and osteoclasts.

MiRNAs are a class of small (20–24-nucleotide) non-coding RNAs that negatively regulate the expression of target gene by inducing degradation of mRNA or repressing its translation [38]. It has been reported that EVs contain abundant miRNAs and can transfer miRNAs to specific cells, where the exogenous miRNAs can regulate the gene expression and biological activity of recipient cells [39]. To clarify the molecular mechanisms of UCB-EVs on osteoblast and osteoclast formation, we performed qRT-PCR to detect the key miRNAs that may function. We previously identified a new miRNA (miR-3960) in osteoblasts, and found that mir-3960 promoted osteoblast differentiation through repressing Homeobox A2, an inhibitor of Runx2 expression [26]. Knockdown of miR-3960 could result in decreased osteoblastogenesis [26]. We also reported that overexpression of miR-3960 induced osteogenic transdifferentiation of vascular smooth muscle cells, whereas inhibition of miR-3960 expression caused an opposite effect [27]. In the present study, we detected high level of miR-3960 in UCB-EVs, and found that UCB-EVs-induced osteogenesis of BMSCs was partly abolished by miR-3960 inhibition, suggesting that miR-3960 is one of the critical molecules in UCB-EVs for stimulating bone formation. However, miR-3960 inhibition could not affect the anti-osteoclastic effect of UCB-EVs, implying other molecules would participate in this process that remain to be further investigated. Studies have shown that the enrichment of contaminating molecules in the isolated EVs is still a controversial issue and high purity isolation methods are required [40,41]. Ultracentrifugation usually obtains pelleted EVs along with non-EV-related molecules [42], and these unspecific substances may influence the real efficacy of EVs, which is another limitation of our study.

In conclusion, our results demonstrate that UCB-EVs are able to ameliorate age-related bone loss in mice. The potential mechanism may be the regulation of function properties of osteoblasts and osteoclasts, as UCB-EVs can promote osteogenic differentiation of BMSCs and inhibit osteoclastic differentiation of osteoclast precursor cells *in vitro*. Furthermore, miR-3960 plays an important role in the influence of UCB-EVs on osteoblast differentiation, since suppression of miR-3960 can markedly reverse the regulatory effects of UCB-EVs. Our data suggest that UCB-EVs may represent a novel therapeutic tool for osteoporosis.

Supplementary data to this article can be found online at https://doi.org/10.1016/j.metabol.2019.01.009.

Author contributions

HX and YH designed the study and drafted the manuscript. YH performed the main part of experiments and analyzed the data. RX, CYC and SSR helped with the *in vivo* experiments. KX, JH, HY, YJT and JL helped with the biochemical experiment. ZXW, JC and ZZL provided technical support. All authors reviewed and approved the manuscript.

Acknowledgements

The study was partially presented as a poster in the 3rd International Chinese Musculoskeletal Research Conference & the 5th International Biomedical Forum of West China, Shihezi 2017.

We thank Kui-Lin Fei and Wen-Yan Jian for their assistance in the collection of the human UCB samples.

Funding

This work was supported by the National Natural Science Foundation of China (Grant No. 81670807, 81871822, 81702237, 81600699, 81701383), the Excellent Young Scientist Award of National Natural Science Foundation of China (Grant No. 81522012), the Thousand Youth Talents Plan of China (Grant No. D1119003), the Hunan Youth Talent Project (Grant No. 2016RS3021), the Innovation Driven Project of Central South University, China (Grant No. 2016CX028, 2019CX014), the Youth Foundation of Xiangya Hospital in Central South University, China (Grant No. 2016Q10), the Fundamental Research Funds for the Central Universities of Central South University, China (Grant No. 2017zzts014, 2017zzts032, 2018zzts895), the Hunan Provincial Natural Science Foundation, China (Grant No. 2017JJ3501), the China Postdoctoral Science Foundation (Grant No. 2017M612596) and the Natural Science Foundation for Distinguished Young Scholars of Guangdong Province, China (Grant No. 2016A030306051).

Competing interests

None.

References

[1] Sheyn D, Shapiro G, Tawackoli W, Jun DS, Koh Y, Kang KB, et al. PTH induces systemically administered mesenchymal stem cells to migrate to and regenerate spine injuries. Mol Ther 2016;24(2):318–30.
[2] Makras P, Delaroudis S, Anastasilakis AD. Novel therapies for osteoporosis. Metabolism 2015;64(10):1199–214.
[3] VanderWalde A, Hurria A. Aging and osteoporosis in breast and prostate cancer. CA Cancer J Clin 2011;61(3):139–56.
[4] Farr JN, Xu M, Weivoda MM, Monroe DG, Fraser DG, Onken JL, et al. Targeting cellular senescence prevents age-related bone loss in mice. Nat Med 2017;23(9):1072–9.
[5] Iacobini C, Blasetti FC, Bedini R, Pecci R, Bartolazzi A, Amadio B, et al. Galectin-3 is essential for proper bone cell differentiation and activity, bone remodeling and biomechanical competence in mice. Metabolism 2018;83:149–58.
[6] Xie H, Cui Z, Wang L, Xia Z, Hu Y, Xian L, et al. PDGF-BB secreted by preosteoclasts induces angiogenesis during coupling with osteogenesis. Nat Med 2014;20(11):1270–8.
[7] Maimoun L, Sultan C. Effects of physical activity on bone remodeling. Metabolism 2011;60(3):373–88.
[8] Conboy IM, Conboy MJ, Wagers AJ, Girma ER, Weissman IL, Rando TA. Rejuvenation of aged progenitor cells by exposure to a young systemic environment. Nature 2005;433(7027):760–4.
[9] Katsimpardi L, Litterman NK, Schein PA, Miller CM, Loffredo FS, Wojtkiewicz GR, et al. Vascular and neurogenic rejuvenation of the aging mouse brain by young systemic factors. Science 2014;344(6184):630–4.
[10] Villeda SA, Plambeck KE, Middeldorp J, Castellano JM, Mosher KI, Luo J, et al. Young blood reverses age-related impairments in cognitive function and synaptic plasticity in mice. Nat Med 2014;20(6):659–63.
[11] Roura S, Pujal JM, Galvez-Monton C, Bayes-Genis A. The role and potential of umbilical cord blood in an era of new therapies: a review. Stem Cell Res Ther 2015;6:123.
[12] Frazier SK, Higgins J, Bugajski A, Jones AR, Brown MR. Adverse reactions to transfusion of blood products and best practices for prevention. Crit Care Nurs Clin North Am 2017;29(3):271–90.
[13] Cid J. Prevention of transfusion-associated graft-versus-host disease with pathogen-reduced platelets with amotosalen and ultraviolet A light: a review. Vox Sang 2017;112(7):607–13.
[14] Tkach M, Thery C. Communication by extracellular vesicles: where we are and where we need to go. Cell 2016;164(6):1226–32.
[15] Lener T, Gimona M, Aigner L, Borger V, Buzas E, Camussi G, et al. Applying extracellular vesicles based therapeutics in clinical trials - an ISEV position paper. J Extracell Vesicles 2015;4:30087.
[16] Qi X, Zhang J, Yuan H, Xu Z, Li Q, Niu X, et al. Exosomes secreted by human-induced pluripotent stem cell-derived mesenchymal stem cells repair critical-sized bone defects through enhanced angiogenesis and osteogenesis in osteoporotic rats. Int J Biol Sci 2016;12(7):836–49.
[17] Zhang J, Liu X, Li H, Chen C, Hu B, Niu X, et al. Exosomes/tricalcium phosphate combination scaffolds can enhance bone regeneration by activating the PI3K/Akt signaling pathway. Stem Cell Res Ther 2016;7(1):136.
[18] Qin Y, Wang L, Gao Z, Chen G, Zhang C. Bone marrow stromal/stem cell-derived extracellular vesicles regulate osteoblast activity and differentiation in vitro and promote bone regeneration in vivo. Sci Rep 2016;6:21961.
[19] Jia R, Li J, Rui C, Ji H, Ding H, Lu Y, et al. Comparative proteomic profile of the human umbilical cord blood exosomes between normal and preeclampsia pregnancies with high-resolution mass spectrometry. Cell Physiol Biochem 2015;36(6):2299–306.
[20] Hu Y, Rao SS, Wang ZX, Cao J, Tan YJ, Luo J, et al. Exosomes from human umbilical cord blood accelerate cutaneous wound healing through miR-21-3p-mediated promotion of angiogenesis and fibroblast function. Theranostics 2018;8(1):169–84.
[21] Lacroix R, Judicone C, Mooberry M, Boucekine M, Key NS. Dignat-George, Standardization of pre-analytical variables in plasma microparticle determination: results of the International Society on Thrombosis and Haemostasis SSC Collaborative workshop. J Thromb Haemost 2013;11:1190–3.
[22] Rao SS, Hu Y, Xie PL, Cao J, Wang ZX, Liu JH, et al. Omentin-1 prevents inflammation-induced osteoporosis by downregulating the pro-inflammatory cytokines. Bone Res 2018;6:9.
[23] Thery C, Amigorena S, Raposo G, Clayton A. Isolation and characterization of exosomes from cell culture supernatants and biological fluids. Curr Protoc Cell Biol 2006:3–22 [Chapter 3].
[24] Hassan MQ, Tye CE, Stein GS, Lian JB. Non-coding RNAs: epigenetic regulators of bone development and homeostasis. Bone 2015;81:746–56.
[25] Chen J, Qiu M, Dou C, Cao Z, Dong S. MicroRNAs in bone balance and osteoporosis. Drug Dev Res 2015;76(5):235–45.
[26] Hu R, Liu W, Li H, Yang L, Chen C, Xia ZY, et al. A Runx2/miR-3960/miR-2861 regulatory feedback loop during mouse osteoblast differentiation. J Biol Chem 2011;286(14):12328–39.
[27] Xia ZY, Hu Y, Xie PL, Tang SY, Luo XH, Liao EY, et al. Runx2/miR-3960/miR-2861 positive feedback loop is responsible for osteogenic transdifferentiation of vascular smooth muscle cells. Biomed Res Int 2015;2015:624037.
[28] Xie Y, Gao Y, Zhang L, Chen Y, Ge W, Tang P. Involvement of serum-derived exosomes of elderly patients with bone loss in failure of bone remodeling via alteration of exosomal bone-related proteins. Aging Cell 2018;17(3):e12758.
[29] Todeschi MR, El BR, Capelli C, Daga A, Patrone E, Introna M, et al. Transplanted umbilical cord mesenchymal stem cells modify the in vivo microenvironment enhancing angiogenesis and leading to bone regeneration. Stem Cells Dev 2015;24(13):1570–81.
[30] Kiernan J, Hu S, Grynpas MD, Davies JE, Stanford WL. Systemic mesenchymal stromal cell transplantation prevents functional bone loss in a mouse model of age-related osteoporosis. Stem Cells Transl Med 2016;5(5):683–93.
[31] An JH, Park H, Song JA, Ki KH, Yang JY, Choi HJ, et al. Transplantation of human umbilical cord blood-derived mesenchymal stem cells or their conditioned medium prevents bone loss in ovariectomized nude mice. Tissue Eng Part A 2013;19(5–6):685–96.
[32] Antebi B, Pelled G, Gazit D. Stem cell therapy for osteoporosis. Curr Osteoporos Rep 2014;12(1):41–7.
[33] Roura S, Pujal JM, Galvez-Monton C, Bayes-Genis A. Impact of umbilical cord blood-derived mesenchymal stem cells on cardiovascular research. Biomed Res Int 2015;2015:975302.
[34] Xu S, Liu C, Ji HL. Concise review: therapeutic potential of the mesenchymal stem cell derived secretome and extracellular vesicles for radiation-induced lung injury: progress and hypotheses. Stem Cells Transl Med 2019;00:1–11.
[35] Zheng G, Huang R, Qiu G, Ge M, Wang J, Shu Q, et al. Mesenchymal stromal cell-derived extracellular vesicles: regenerative and immunomodulatory effects and potential applications in sepsis. Cell Tissue Res 2018;374(1):1–15.
[36] Furuta T, Miyaki S, Ishitobi H, Ogura T, Kato Y, Kamei N, et al. Mesenchymal stem cell-derived exosomes promote fracture healing in a mouse model. Stem Cells Transl Med 2016;5(12):1620–30.
[37] Li CJ, Cheng P, Liang MK, Chen YS, Lu Q, Wang JY, et al. MicroRNA-188 regulates age-related switch between osteoblast and adipocyte differentiation. J Clin Invest 2015;125(4):1509–22.
[38] Li H, Xie H, Liu W, Hu R, Huang B, Tan YF, et al. A novel microRNA targeting HDAC5 regulates osteoblast differentiation in mice and contributes to primary osteoporosis in humans. J Clin Invest 2009;119(12):3666–77.
[39] Au YC, Co NN, Tsuruga T, Yeung TL, Kwan SY, Leung CS, et al. Exosomal transfer of stroma-derived miR21 confers paclitaxel resistance in ovarian cancer cells through targeting APAF1. Nat Commun 2016;7:11150.
[40] Gamez-Valero A, Monguio-Tortajada M, Carreras-Planella L, Franquesa M, Beyer K, Borras FE. Size-exclusion chromatography-based isolation minimally alters extracellular vesicles' characteristics compared to precipitating agents. Sci Rep 2016;6:33641.
[41] Monguio-Tortajada M, Roura S, Galvez-Monton C, Pujal JM, Aran G, Sanjurjo L, et al. Nanosized UCMSC-derived extracellular vesicles but not conditioned medium exclusively inhibit the inflammatory response of stimulated T cells: implications for nanomedicine. Theranostics 2017;7(2):270–84.
[42] Konoshenko MY, Lekchnov EA, Vlassov AV, Laktionov PP. Isolation of extracellular vesicles: general methodologies and latest trends. Biomed Res Int 2018;2018:8545347.